Automated Defect Detection and Classification in Ashlar Masonry Walls using Machine Learning

Automated Defect Detection and Classification in Ashlar Masonry Walls using Machine Learning

E. Valero[a*], A. Forster[b], F. Bosché[a], E. Hyslop[c], L. Wilson[c] and A. Turmel[c]

[a]Institute for Infrastructure and Environment, School of Engineering, The University of Edinburgh, Edinburgh EH9 3FB, UK
[b]Institute for Sustainable Building Design, Heriot-Watt University, Edinburgh EH14 4AS, UK
[c]Historic Environment Scotland, Salisbury Place, Longmore House, Edinburgh EH9 1SH, UK

*Corresponding author: Enrique Valero, e.valero@ed.ac.uk

Abstract

Methods employed for surveying buildings for condition have traditionally been reliant upon visual assessment and manual recording. Survey of traditional masonry also ostensibly conforms to this approach but, due to the sheer volume of masonry units composing walls, it is often prohibitively time consuming, exceptionally complex and ultimately costly. Notable features of such survey work for ashlar stone types require each stone to be labelled and overlaid with information relative to condition. Further hindering these already costly operations, it has been shown that the accuracy of reporting, including labelling the manifestation of defects and defect diagnosis, is subjective, depending upon the expertise and experience of those evaluating the fabric. Moving beyond these preliminary survey and reporting stages, this situation gives rise to variable repair and maintenance strategies that can have significant cost implications and can debase fundamental conservation activities.

The development of digital technologies, such as terrestrial laser scanning, and advancements in novel computer vision statistical techniques can help produce accurate representation of buildings that can be subsequently rapidly processed, achieving many tangible survey functions with greater inherent objectivity. In this paper, an innovative strategy for automatic detection and classification of defects in digitised ashlar masonry walling is presented. The classification method is based on the use of supervised machine learning algorithms, assisted by surveyors' strategies and expertise to identify defective individual masonry units, through to broader global patterns for groups of stones. The proposed approach has been tested on the main façade of the Chapel Royal in Stirling Castle (Scotland), demonstrating its potential for ashlar masonry forms of wall construction. It is important to recognise that the findings are not limited to this culturally significant building and will be of high value to almost innumerable ashlar-built structures worldwide. The research ultimately attempts to reduce the degree of subjectivity in classifying defects, on a scale and rapidity hitherto beyond traditional project cost constraints. Importantly, it is recognised that through automation more effective utilisation of resources that would have been traditionally spent on survey can be redeployed to support fabric intervention or routine maintenance operations.

Keywords

surveying, digital reality capture, masonry defects, machine learning

1 Introduction

1.1 Survey Objectivity, Cost and Efficiency

Repair and maintenance operations are essential for the effective and efficient performance and in-service use of buildings. Maintenance is so fundamentally important in attaining conservation objectives that it has been enshrined into all international charters for best practice intervention strategies [1] and wider building operations. Indeed, an absence of maintenance is well understood to result in accelerated decay in historic building fabric and corresponding loss of imbued cultural significance [2] [3]. Fundamental to these processes are survey and reporting for various purposes, most common of these is arguably survey for condition that acts as a starting point for many other processes.

Traditional methods employed for surveying buildings for condition have been reliant upon visual assessment and manual recording that have been shown to be frequently variable in outcome [4] [5]. Survey of traditional ashlar masonry conforms to this approach but, due to the sheer volume of masonry units composing the walls, it is frequently extremely time consuming and costly. In terms of the practical replacement of dimensional stone it is essential that each stone must be labelled and overlaid with geometric information and, most importantly, accurate stone sizing. For those stones that are to be conserved as opposed to replaced, information relative to condition is required to support repair strategy decision making. Compounding issues surrounding these time intensive operations, it has been shown that the accuracy of data produced, reporting structure, and determination of defect manifestation through to diagnosis, are subjective depending upon the expertise of the surveyor.

The implication of misclassification of defects manifestations can result in inaccurate diagnosis and prognosis. Practically, these inaccuracies have resulted in incorrect repair strategies and remedial treatments that have been costly to reverse or have accelerated fabric decay debasing fundamental conservation activities they purport to engender. To understand the probability of misappropriation of the manifestation of defects, it is important to recognise the general level of education in surveying and architecture that supports decision making in this area. Indeed, it is not uncommon to find 'relatively inexperienced professionals "grappling" with complex specification and design issues, within the context of short time frames' [5]. This situation is therefore prone to error, and Forster and Douglas [5] have called for greater "early stage involvement of a specialist masonry contractor […] reducing inaccuracies in specifications and working method statements for lime and masonry works". Such an integrated approach to masonry survey, in which both professional surveyors and specialist masonry contractors work in unison, would create an environment for better reporting due to collective expertise. However, given the increased professional survey cost of such an approach, automatic detection of defects in precise digital models created from the laser scanning of masonry works, offers the promise of a paradigm shift in accuracy and financial efficiency in operations.

1.2 Digital Reality Capture

Beyond variability in reporting, the efficiency in survey productivity is hindered by the time-consuming data acquisition of traditional visual survey and the cost associated with safe access for inspection. Visual survey and detailed production of what were ostensibly hand-drawn elevations required to

facilitate these operations are prohibitively costly (even when the drawing is conducted from rectified pictures) and constitute a significant proportion of the project budget.

Within this context, the rapid evolution of reality capture technologies has facilitated the representation of different environments in either printed or digital formats [6]. Among these devices, photographic cameras have been conventionally employed to produce instantaneous 2D illustrations and, more recently, photogrammetric techniques (e.g. structure from motion (SfM)) have been developed to create realistic three-dimensional models of objects and spaces from sets of pictures acquired by digital single-lens reflex (DSLR) cameras [7].

Simultaneously, with the improvement of cameras, laser scanning technology has been developed that is able to comprehensively, accurately and rapidly capture the geometry of the surrounding environment. Laser scanning delivers precise 3D data in the form of point clouds and is more accurate and rapid than photogrammetry. However, colour information obtained from DSLR cameras is, in general, more reliable than colour information obtained from cameras commonly built in many laser scanners [8].

Even though numerous authors have applied these technologies in the field of heritage, for visualisation purposes (e.g. [9]) or the generation of historic building information modelling (HBIM) models [10], more research is needed on the application of reality capture technologies and subsequent data processing to transform traditional surveying strategies, to produce more objective results in faster and more cost-effective ways.

2 Literature Review

2.1 Building Pathology: Stone Defect Ontology

Failure to achieve an accurate and common understanding of reported defects and their prognosis can result in confusion and often insensitive interventions debasing conservation effectiveness. Aiming to deliver more general definitions of defects, deterioration of building fabric can be classified into any one, or a combination of universal agents of change and subsequent degradation processes. Pragmatic contextualisation of these degradation processes for masonry has traditionally been grouped within 5 primary factors, as illustrated in Table 1.

Within these broad groupings are numerous specific sub-groups for the wide-ranging defects that may be encountered. Most recently, these have been effectively contextualised, categorised and defined in the ICOMOS '*Glossary on Stone Deterioration Patterns*' [11]. This internationally developed document aims to transcend national terminology and create universally accepted masonry defect definitions and labelling. The sub-groupings include: cracks, discolouration, mechanical damage, erosion, delamination, crusts and biological growth. These in turn can be mapped effectively onto the former outlined broad primary degradation factors (see Table 1).

In this paper, we also utilise these definitions proposed by ICOMOS. The defects that form the basis of the study reflect the broad groupings and are representative of defects in ashlar masonry that commonly confront surveyors.

Table 1: Masonry defects: Manifestation, identification and diagnosis

Primary degradation factors / agents of change	ICOMOS stone defect classification	Manifestation, Identification and Diagnosis
Stress factors	Cracks	*Structural movement - global:* Rotation of wall faces / out of plumb. Buckling of walls. Evaluation of planar surfaces; Inconsistencies in level / plumb / deflection. Cracks associated with structural movement – differential and uniform settlement.
		Structural movement – local: Load path alteration and force redirection leading to localised stress concentration (overloading) in masonry and mortars. Both compressive and tensile fracturing in materials associated with overloading – stress concentration especially in fenestration, buttresses and piers etc. Tensile fractures associated with movement. Fundamental importance of size, location and shape of fractures and whether they are compressive or tensile in nature. Additionally, it is important to ascertain whether the movement is progress or static. Analysis of fracture / crack patterns as a primary mechanism for supporting pathology / prognosis and diagnosis.
		Movement associated with materials moisture and or thermal fluctuations.
		Volumetric instability and movement associated with chemical reactions and responding materials change / conversion. Ferrous fixings corroding and causing expansive forces in masonry – fracturing and 'blowing' faces off stone.
Weathering factors	Material loss - Erosion: Fabric loss of masonry units	Friable materials, surface dissolution, alveolisation (Honeycombing), voids, recessed materials, faces blown in brickwork, etc. Large or small magnitude spalling events.
	Material loss - Erosion: Fabric loss in pointing and bedding mortars	Undercutting of masonry unit. Increased prevalence of moisture ingress and penetrating dampness at depth. Deterioration from original pointing finish / wall line. Binder migration in lime mortars and wall core voiding.
	Detachment - Delaminating, scaling and peeling in natural stone	Face bedded stone ('on cant'– deterioration along bedding planes), contour scaling, fabric detachment.
Incompatibility factors	Discolouration	Contaminated masonry: Efflorescence and crypto-efflorescence salt blooms, salt crystallisation deterioration and surface dissolution. Crusts and blisters associated with pollutants.
		Contaminated masonry via surface water runoff such as copper roofing materials and iron oxide staining from in built ironwork. Volumetric instability and movement associated with chemical instability and responding materials change / conversion – ferrous fixings in stone.
		Crusts & Discoloration – both from internal and external environment (NO_x and SO_x pollutants) and hydrocarbon sulphate deposits (SO_x) from unlined chimneys etc.
Biological factors	Biological activity	Moulds, slimes, and moss growth often consistent with high and sustained moisture contents, low potential evaporation and an absence of direct sun light. Lichen growth and surface interaction causing localised surface deterioration.
Use factors	Material loss - Mechanical damage	Mechanical damage; vandalism; inappropriate use of masonry elements and components; poor quality installation and maintenance operations.

2.2 Processing Reality Capture Data for Supporting Surveyors

Today, the introduction of novel strategies, grounded on the use of reality capture technologies and data processing techniques, offers opportunities for greater levels of objectivity in reporting the manifestation of masonry condition. In recent years, research has been performed on the use of reality capture technologies to facilitate the work of building surveyors. Conservation of historic structures has received particular attention [12], due in part to these forms of construction having complex and non-standardised structural components which are commonly deteriorated relative to age. Accurate point clouds have been shown to be used effectively for the generation of 3D models and further structural analysis [13, 14], including through Finite Element Analysis [15].

Furthermore, advances in multi-spectral research utilised in conjunction with reality capture have facilitated architectural and archaeological analysis in the attainment of hidden features of structures. Bruno et al. [16] presented a novel approach merging stereo-imaging and structured-light sensing to conduct underwater surveys and Temizer [17] evaluated how the filtering of points affects the accuracy of the mesh generated after the scanned data. The integration of these two techniques is motivated by the difficult survey conditions and underlying complexity (both water visibility and conditions of the artefacts) that can be encountered in underwater exploration. More recently, reality capture data have been utilised for the generation of HBIM models, which can facilitate keeping structured records on defects, and maintenance operations. For example, Anton et al. [18] combine both optical (OS) and Terrestrial Laser Scanners (TLS) to produce accurate building information models that can be subsequently used for evaluating the quality of the produced complex geometries. This complexity of Scan-to-HBIM tasks has encouraged the generation of parametric models and libraries containing architectural elements [19].

The previous paragraphs illustrate that research on the use of reality capture data has focused mainly on visualisation and/or generation of 3D or HBIM models. These processing tasks are usually associated with a series of manual operations that require significant time and user interaction. Moving forward, automation of a variety of processing operations would further facilitate the work of surveyors in their attempts to attain greater objectivity and consistency in results. A prominent example of such automation includes work by Pochtrager et al. [20] who developed a novel strategy for the generation of 3D models of historic wooden roof structures through the automated processing of geometric data from TLS. This method delivers accurate models even if the point clouds produced by the scanners are incomplete. Additionally, Cappellini et al. [21] proposed a semi-automatic approach to semantically label 2.5D data (colour and depth information) for the stratigraphic analysis of masonry walls obtained by means of photogrammetric techniques. This facilitates subsequent repair and maintenance tasks. Research of this nature has been further developed by Bosche, Valero and Forster [22, 23] who wrote bespoke algorithms for the automatic segmentation of individual masonry units. These works have been produced in support of survey and evaluation of historic fabric on a finer level of detail, enabling the subsequent improvement in inspection, diagnosis, and repair decisions-making [24].

In addition to traditional data processing approaches, novel techniques based on artificial intelligence, both supervised or unsupervised, have recently attracted interest. Oses and Dornaika [25] proposed a semi-automatic delineation and masonry classification by means of k-NN classifiers to identify stone blocks in 2D images. Whilst, Armesto et al. [27] focused on the inspection of structural pathologies suggesting the use of the fuzzy k-means algorithm to identify and map ashlar affected by moisture. And recent work by Sánchez et al. [27] proposed a novel strategy, based on the CANUPO classifier, to

identify in point cloud data deformation and erosion of walls and highlight unit clusters (i.e. areas) affected by decay.

2.3 Contribution

Taking advantage of the speed and accuracy of modern reality capture data technologies presented above, this paper outlines a novel approach to automatically detect defective patterns in masonry walls by means of Machine Learning (ML) techniques and algorithms.

Learning from traditional surveying strategies, which rely on the visual inspection of structural elements by expert surveyors, this new method is devoted to enhancing the reliability of current (i.e. manual/visual) techniques, by automating both defect detection and classification processes to deliver more reliable outcomes. Even though the learning/training process of the designed algorithms is built on results from traditional surveys (through training data labelling), manual input is required only for initial ML training, as opposed to recurrently for every survey. This digital strategy creates opportunities for faster, more cost-effective and objective repair and maintenance and offers the prospect of redirecting limited financial resources toward higher value operations.

Whilst several authors have previously worked on the detection of contaminated masonry and biological activity (e.g. [26] and [27]), this work is also devoted to the detection and classification of several primary defects related to the loss of material, such as mechanical damage, erosion and delamination. Furthermore, a seemingly minor aspect of any masonry project is the 'first order' requirement to locate the position of individual defective masonry units. This is critical for many processes that flow from this classification. Primary operations commonly encountered are: the replacement or consolidation of ashlar stone and objective quantification of these targeted interventions, and the accurate estimation of specified materials. A novel and more precise analysis of fabric at different levels of detail (as presented in [23, 24]) is performed here. The segmentation of masonry into ashlar units presents several advantages with respect to previous works (e.g. [27]) where more extensive areas are considered for defect analysis. First, this facilitates a unit-level survey of wall elements to be included in BIM models, delivering information about a particular stone that can be monitored over time, which is useful for repair and maintenance works. Second, a more accurate analysis is provided, since global flatness control is complex in the case of historic buildings.

3 Proposed Approach

As previously stated, the aim of this work is the automatic identification of defective areas in digitised masonry ashlar walls and the further classification of these regions according to different decay patterns. Prior to these operations, as illustrated in Figure 1, a precise and coloured 3D point cloud of a wall is produced. This dataset, containing geometric and colour information, is obtained by the combination of two different point clouds delivered by a laser scanner and photogrammetry. While precise 3D coordinates are acquired by the scanner, accurate colour is provided by a point cloud generated through Structure from Motion from photographs taken by a DSLR camera. From this pre-processed point cloud, ashlar units are subsequently automatically segmented, following a novel approach grounded on the use of the 2D Continuous Wavelet Transform to identify the joints between units [23]. Segmented ashlar stones are afterwards processed and different regions of interest (ROI), containing potentially defective areas, are automatically retrieved and highlighted. Finally, these ROI

are processed by means of an algorithm based on machine learning techniques, and decayed areas affected by both colour- and geometry-related defects are accordingly classified.

In the following subsections, all these operations succinctly mentioned above are presented in detail.

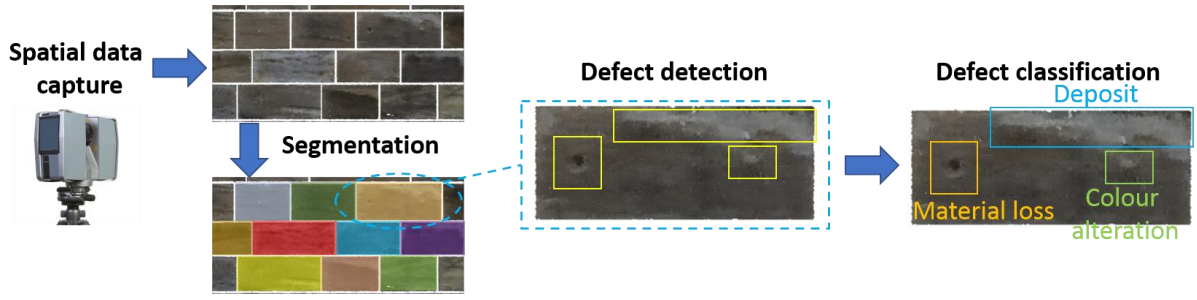

Figure 1: Proposed methodology for defect analysis

3.1 Data acquisition

As discussed in the literature review, cutting-edge remote sensing technologies have been rapidly evolving within the last decade. Amongst those, TLS devices and DSLR cameras have been increasingly used for reality capture in the field of built environment. These non-contact technologies facilitate non-destructive evaluation of the fabric, delivering accurate and precise geometric and colour-related data that can be processed to obtain meaningful information.

TLS technologies can provide large amounts (up to 1Mpts/s) of accurate data (in the order of mm). Point clouds obtained by these devices are more accurate than the ones produced with photogrammetric (PG) techniques, using, as a base, pictures taken by DSLR cameras at several metres from the target [8]. Additionally, photogrammetric outcomes need to be scaled to actual dimensions. In contrast, the colour information delivered by cameras mounted on TLS devices is, in some cases, limited by the area coverage of the cameras and the quality of the embedded cameras [28].

Therefore, in this work, both technologies (TLS and PG) are combined to produce accurate point cloud coloured with reliable Red-Green-Blue (RGB) information. In order to create these precise models, both point clouds were aligned and, subsequently, each point from the TLS cloud was coloured with the RGB information from its nearest neighbour from the PG model.

3.2 Data segmentation

After pre-processing the raw data, obtained by TLS and PG, an additional operation is required to deliver a high level of detail (LoD) analysis of the decay on stone surfaces: the segmentation of ashlar units. This operation facilitates the division of building *elements* (walls, in this case) into simpler components, named *units*, and supports the study of defects at different LoD, from elements to sub-unit regions [24]. The segmentation of masonry units, which is not the subject of this paper, is based on the 2D Continuous Wavelet Transform (CWT). This operation is applied to the coloured 3D data of a wall, as detailed in [23], to identify joints between masonry units and segment single stones.

3.3 Detection of manifestations of defects

As a first approach to detect and highlight areas containing defects, segmented individual ashlar units are evaluated to identify regions potentially affected by deformation or loss of material and chromatic alterations. For this detection process, two characteristics are initially assumed: surfaces of ashlar units are relatively (1) flat and (2) homogeneous in colour. Therefore, rougher or discoloured areas are considered outliers and are thoroughly analysed to identify defects.

3.3.1. Geometric defects

The homogeneity (or heterogeneity) of geometry and colour attributes can be defined by means of mathematical tools. Firstly, and regarding deterioration associated to geometry, a plane is fitted to the surface of each ashlar stone. Areas containing *outliers*, characterised as being points not lying on the plane, are considered potentially affected by decay.

In the case of ashlar masonry walls, units usually present relatively flat surfaces, even if their finishing may differ (e.g. tooled, dragged or polished and rubbed). Therefore, the surface of the ashlar unit (and/or a masonry wall region) should generally fit a plane. Points that are found to be far from the surface plane, called outliers, can be considered as potentially defective regions (see Figure 2a and b). Depending on the finishing of the ashlar, a threshold (i.e. distance point to plane) is set to identify the outliers. The depth of tooling varies depending upon style and materials form. Warland [29] states of tooled surfaces that they "are left with regular chisel marks cut vertically across the surface of the stone […]. These chisel marks are usually specified as so many to the inch". Warland, highlights the occasional use of specialist finish treatments such as 'furrowed surfaces' that are overtly stipulated as 'small flutings from 1/4'' (6.36mm) to 3/8'' (9.5mm) wide are worked vertically or horizontally across the surface'. Out with these overtly specified treatments tooling (or batted) depth is normally below 2.5mm. Coarse surfaces have higher thresholds while smooth ones have lower limits. The layout of these outlying points and how the regions are connected can subsequently help identify the nature of the defects.

Each masonry unit may present one or more defect. To detect different decayed areas, a binary map, with a resolution of 1mm, is created by projecting the above outliers onto the fitted plane, as illustrated in Figure 2c. Note that if two or more points are projected on the same pixel, an average value for depth is considered.

Compact regions, with a surface over 500mm^2, are then segmented from one another using a region growing algorithm. Finally, the original 3D points corresponding to each detected defective area can correlate, as shown in Figure 2d. The segments, enclosed by bounding boxes (i.e. ROI), are stored as independent entities for which geometry-related metrics are subsequently calculated to characterise the deterioration patterns.

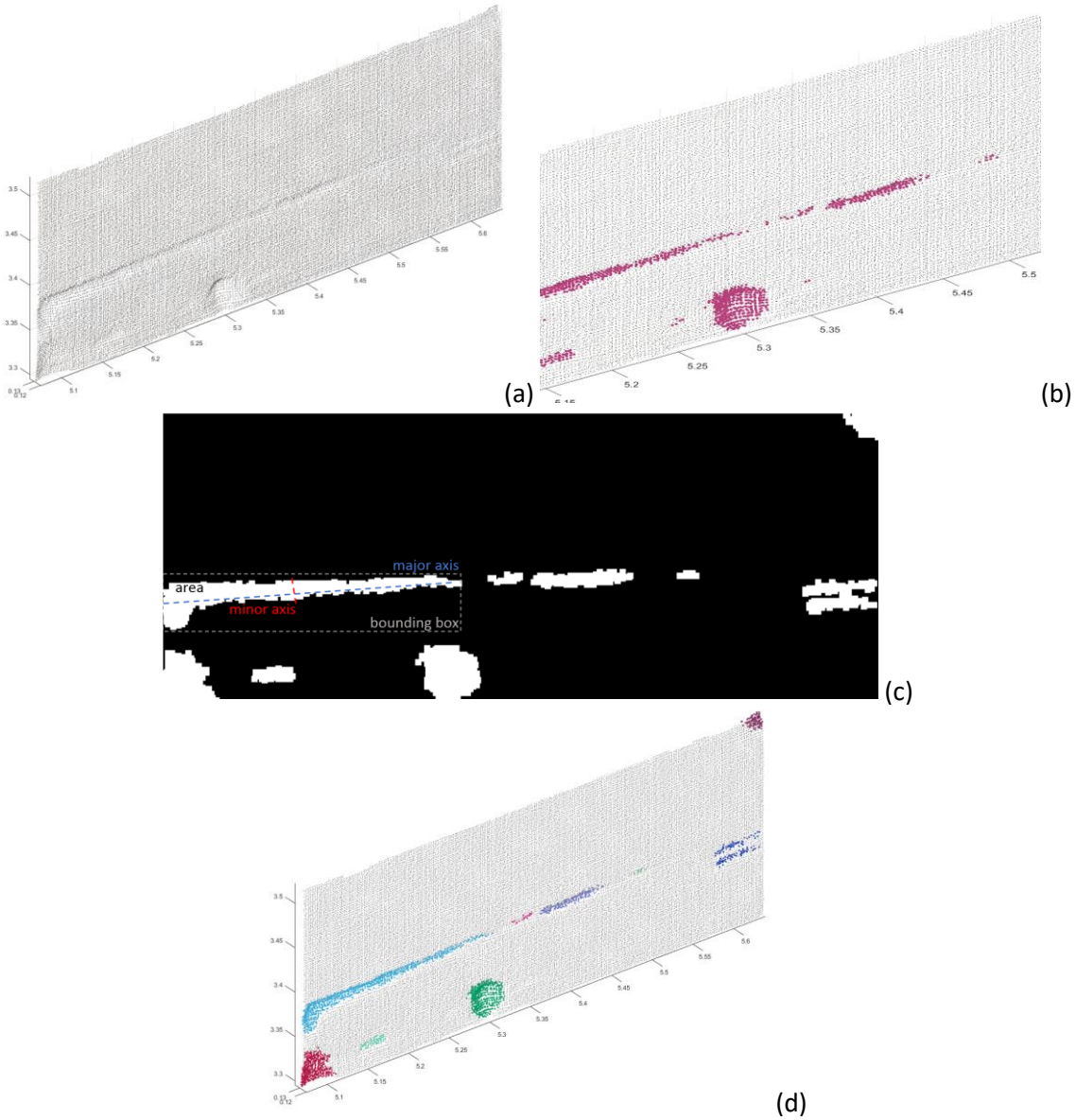

Figure 2: Process for the extraction of geometric parameters. a) Point cloud of an ashlar masonry wall. b) Outliers, highlighted in pink. c) Binary map after orthogonal projection of outliers. d) Potential geometry-related defective areas highlighted in different colours. In subfigures including axes, values are in meters.

3.3.2. Chromatic alterations

With respect to chromatic alterations and potential colour-related defective areas, a similar approach, based on the extraction of outliers is proposed. In this case, regions with some colour components far from the average are potentially defective and are highlighted to be used as inputs in the subsequent classification process.

Colour information is usually delivered and presented under the RGB format. However, for colour comparison purposes, other models that better align with human colour perception may be preferable [30]. That is the case of the Hue-Saturation-Value (HSV) model, which is used in this paper. This model facilitates the analysis of the predominant *hues* (h) in stones as well as the evaluation of darker and lighter areas, by means of the *value* (v) channel. These two parameters, hue and value, play an important part in the study of colour alterations in stones, and several metrics can be calculated from them.

Following the RGB-to-HSV colour transformation using the approach in [31], the patterns of distribution of colour on each stone, at sub-stone level, or between stones, are evaluated. More precisely, the mean and standard deviation of the *v* channel are calculated to detect *outlier* regions. As an example, areas with a value component over $\mathrm{mean(v)} + \mathrm{std(v)}$ are plotted in cyan in Figure 3b, while points whose value is under $\mathrm{mean(v)} - \mathrm{std(v)}$ are highlighted in dark blue.

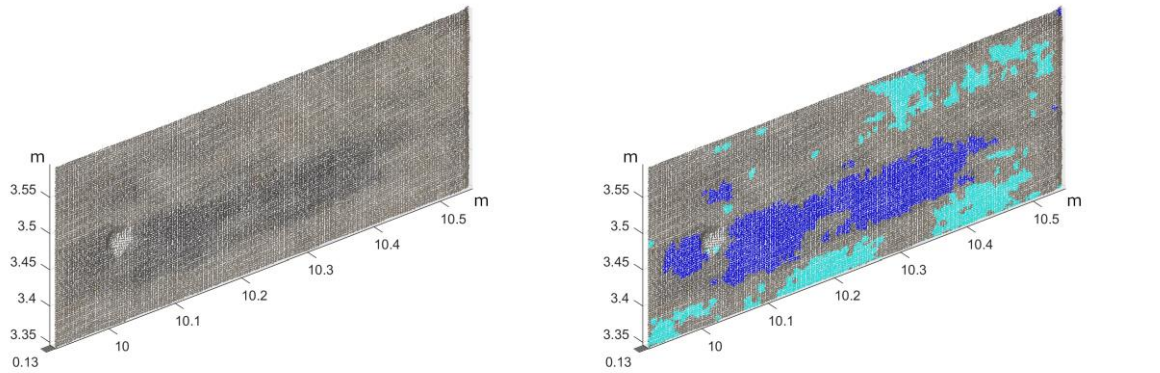

Figure 3: Areas with value components beyond a defined threshold. a) Original point cloud. b) Light areas in cyan and dark areas in blue

3.4 Defect Classification - Parameters defining material change

For the purpose of machine learning techniques, the objective assertion of simple 'changes' in fabric from the surface is all that can be expressed or objectively reported. Diagnosis requires additional data inputs to target the likelihood of causal relationships to any particular defect.

Stone decay often manifests itself through alterations in the geometry and surface textures of the masonry units or the colour of their surface. Both 3D and RGB data, obtained with reality capture devices, can be processed to codify and quantify changes in material using different mathematical operations (i.e. parameters) which can be used to detect and classify masonry defects.

A number of materials change parameters are selected for utilisation and gathered into two groups:

- *geometry-related parameters*, evaluating the deviation of the masonry surface to the expected original profile;
- *colour-related parameters*, linked to colour alterations on the stone;

It is noted that, in both colour and geometry groups, *texture-related parameters* were considered, which are devoted to the study of repetitive patterns within the Region of Interest (ROI). This ROI can be a whole ashlar unit or a sub-unit (i.e. part of a stone) region.

3.4.1 Geometry-related Parameters

Deterioration parameters related to geometry can capture either the relationship between points within the segment (i.e. bounding box), and/or their location with respect to the ashlar surface. In this work, the following parameters are considered:

- **Ratio of outliers over inliers** within the ROI, which can highlight the severity of the defect.

- **Roughness** (RaO) is a geometric characteristic that measures the irregularity of an area. It can highlight those areas affected by material loss or deformation. A roughness coefficient is calculated as the standard deviation of the distances of the *outliers* to the profile's fitted plane (Eq. 1):

$$RaO = \sqrt{\frac{1}{N}\sum_{i=1}^{N}(d_i - \mu)^2}, \text{ with } \mu = \frac{1}{N}\sum_{i=1}^{N} d_i \quad (1)$$

  where N is the number of outliers for the given ROI (stone face or face sub-region), and d_i is the projection distance of the i^{th} point to the fitted plane. Note that the roughness coefficient (*Ra*) can also be calculated for all the points inside the ROI bounding box, i.e. both inliers and outliers.
- **Median distance** from the outliers to the fitted plane for each segment.
- The **distribution of normal vectors** is characterised by the median and standard deviation of the normal vectors of the outliers within a segment (with respect to the overall ashlar surface normal), delivering information about the shape (i.e. variation in orientation) of decayed regions.
- The **area** covered by outliers for each segment (calculated using the 2D map; see Figure 2c).
- The **elongation** (E) of each segment, which is calculated as the fraction of the length of the minor axis of the defective segment divided by the major one (Eq. 2). This metric determines how 'oblong' defective areas are.

$$E = \frac{minor\_axis}{major\_axis} \quad (2)$$

- The **rectangleness** of each defective region, which corresponds to the fraction of the bounding box covered by the projection of the 3D points. It should be noted that the bounding box can be defined as the minimum rectangular area that comprehends the projection of the defect.
- The **circularity** (C) of the decayed region, calculated as the ratio of the area of the projection of the defective region to the area of a circle with the same perimeter (p), as illustrated in Eq. 3.

$$C = \frac{4 \cdot area \cdot \pi}{p^2} \quad (3)$$

- The **number and area of unconnected defective areas** (white segments in Figure 2c) within each ashlar unit. Note that this parameter is applied only to ROIs that are entire units.

3.4.1.1 3D Texture

In addition, geometric texture related features deliver information about the spatial distribution of depth variation in an ROI. In this paper, the study of texture is based on the idea presented by Haralick et al. [32] for image classification. Point clouds depicting ashlar units are orthogonally projected onto a plane which fits the face of the stone as previously detailed, generating a depth map.

Several feature vectors can be obtained by analysing the relation between pairs of pixels in that 2D map, i.e. second order statistics. Different to first order statistics, which deliver properties about individual pixels (e.g. average, standard deviation), second-order and higher statistics estimate properties of several pixels at specific location relative to each other.

Second order statistics can be evaluated to create co-occurrence matrices (CM) which deliver information about how often a pixel with value *i* is adjacent to a pixel with value *j*, where $i, j \in [n] = \{1, \dots, L\}$, with L the levels of depth present in the images [33]. Once calculated, the co-occurrence matrices are processed to obtain various texture features:

- **Contrast** illustrates the variation of intensity (here depth) between a particular pixel and its neighbours over the ROI and is defined by Eq. 4.

$$contrast = \sum_{i=1}^{L}\sum_{j=1}^{L}|i-j|^2 \cdot CM(i,j) \quad (4)$$

- **Energy** calculates the sum of squared elements in CM and indicates the variation of intensity in the region:

$$energy = \sum_{i=1}^{L}\sum_{j=1}^{L} CM(i,j)^2 \quad (5)$$

- Looking for relationships in the ROI, **correlation** measures the linear dependence between pixels at the specified positions relative to each other:

$$correlation = \sum_{i=1}^{L}\sum_{j=1}^{L}\frac{(i-\mu_i)(j-\mu_j)CM(i,j)}{\sigma_i\sigma_j} \quad (6)$$

where $\mu_k = \sum_{i=1}^{L}\sum_{j=1}^{L} k \cdot CM(i,j)$ and $\sigma_k = \sum_{i=1}^{L}\sum_{j=1}^{L}(k-\mu_k)^2 \cdot CM(i,j)$, with $\mathrm{k} = \{\mathrm{i},\mathrm{j}\}$

- **Homogeneity** measures the closeness of the distribution of elements in the CM to its diagonal:

$$homogeneity = \sum_{i=1}^{L}\sum_{j=1}^{L}\frac{CM(i,j)}{1+|1-j|} \quad (7)$$

Table 2 shows examples of various stone depth maps along with the values of 3D texture parameters obtained for them. Note that, in depth maps, darker colours represent shallow regions, while brighter shades correspond to deep areas.

Table 2: Texture features for two potentially defective areas

Depth map	Contrast	Correlation	Energy	Homogeneity
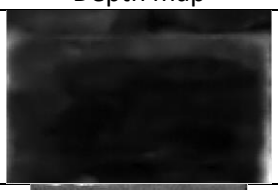	0.06	0.93	0.53	0.97
	0.23	0.62	0.39	0.88
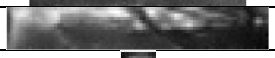	0.40	0.93	0.09	0.83
	1.45	0.81	0.04	0.61

3.4.2 Colour-related Parameters

The metrics above support the identification of defects related to deformation or loss of material. However, other information is required for the detection and classification of areas affected by chromatic alterations, such as discolouration, deposit and biological colonisation (see [11]).

Ashlar units containing outlier areas in the *v* or *h* channels are further investigated with the following parameters calculated:

- **Dispersion of hue**, by means of the calculation of the standard deviation of hue values in each ashlar unit:

$$H_\sigma = \sqrt{\frac{1}{N}\sum_{i=1}^{N}(h_i - \mu)^2}, \text{ where } \mu = \frac{1}{N}\sum_{i=1}^{N} h_i \quad (8)$$

- **Dispersion of value**, by means of the calculation of the standard deviation of value components in each ashlar unit:

$$V_\sigma = \sqrt{\frac{1}{N}\sum_{i=1}^{N}(v_i - \mu)^2}, \text{ where } \mu = \frac{1}{N}\sum_{i=1}^{N} v_i \quad (9)$$

- **Range of hue**:

$$\max(h_i) - min(h_i) \quad (10)$$

- **Range of value**:

$$\max(v_i) - min(v_i) \quad (11)$$

3.4.2.1 Colour Texture

Texture parameters associated to the colour information of the point cloud representing an ROI can be analysed similarly to geometric information. In the case of colour, texture parameters are calculated by using two maps: a colour map (using the HSV model), and a grayscale image calculated from the RGB values using the approach in [31].

Here again, parameters can be considered that simply analyse the values of each channel and how they are distributed in a histogram (first order statistics) or evaluate the relation between pairs of pixels (second order statistics).

- **Skewness** [34] measures the asymmetry of the probability distribution. In the case of the colour of stones, indicating to what extent the intensity values across the overall area vary from the average value. Skewness is calculated using the grayscale image as follows:

$$\gamma_3 = \frac{\frac{1}{N}\sum_{i=1}^{N}(g_i-\mu)^3}{\sqrt{\frac{1}{N-1}\sum_{i=1}^{N}(g_i-\mu)^2}^3}, \text{ where } \mu = \frac{1}{N}\sum_{i=1}^{N} g_i \quad (12)$$

If $\gamma_3 > 0$ (positive skew), there is a prevalence of darker pixels and if $\gamma_3 < 0$ (negative skew), there is a prevalence of lighter pixels. Figure 4 illustrates the extraction of the skewness parameter for two ashlar units.

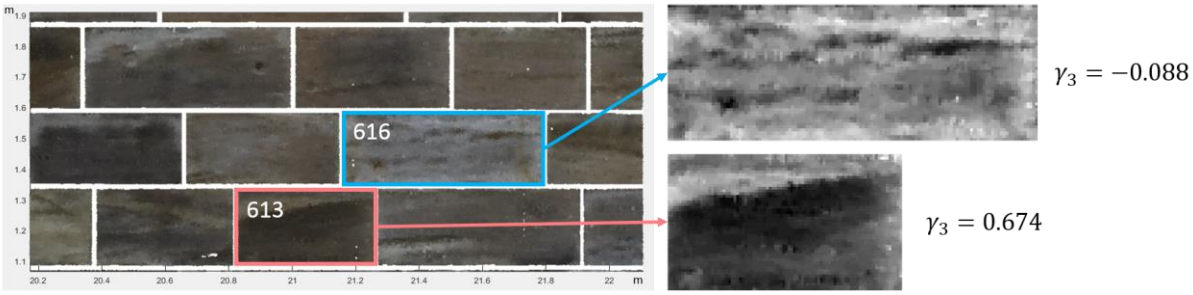

Figure 4: Skewness values for two ashlar units.

Second order statistics are calculated for each channel (i.e. hue, saturation, value and grayscale) as detailed in Section 3.4.1.1 for: contrast (Eq. 4); energy (Eq. 5); correlation (Eq. 6) and homogeneity (Eq. 7). This produces 16 parameters.

3.5 Defect Classification - Machine Learning Algorithm

Similar decayed regions will present common ´symptoms´, with some of the parameters in Section 3.4 displaying comparable values. As a result, the representation of *n* parameters in an n-dimensional space is expected to show different data clusters which can be associated to analogous defects. To determine precise boundaries between these clusters, machine learning techniques are used in this paper.

The selection of an adequate machine learning approach depends on the number and nature of samples in the studied dataset and evaluated features [35]. In this work, after considering the number of available samples (around 3,000 for both geometric and colour analysis) and the extracted features (less than 20 in both cases), a supervised technique, more precisely a logistic regression multi-class classification algorithm, has been employed to categorise defective areas.

For training the supervised classifier, deteriorated regions have been manually segmented and labelled by experienced building surveyors who specialise in stone, and following the criteria presented by ICOMOS [11] (see Figure 5). Each segment, which is marked as a rectangular ROI, contains a label indicating the defect or defects observed in the area. The selected defect parameters described in Section 3.4 are then calculated using XYZ and RGB data contained within each rectangular boundary.

Training is conducted using a one-vs-all strategy and data from the Chapel Royal façade (that dataset is presented in Section 4), which presents significant geometric and/or colour deviations.

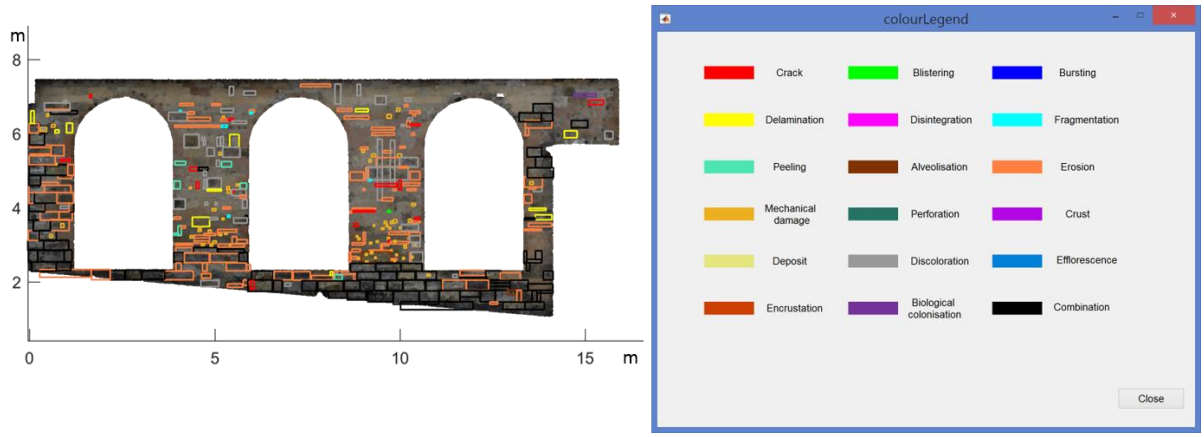

Figure 5: Defective areas labelled by surveyors.

3.5.1 Selection of reliable parameters

Although a number of parameters have been found to be potentially relevant to the detection and classification of stone defects, in practice a subset of those can be found to result in simpler, faster and even more accurate classification. To identify which combination of parameters (or features) provides the most accurate results, the strategy illustrated in Figure 6 is applied separately to geometry and colour-related parameters.

For each possible combination of metrics, the one-vs-all logistic regression algorithm is subsequently trained and tested for L values (L=5 in this paper), of λ (i.e. regularisation parameter). For every labelled sample, the different combinations of metrics previously established are used as features. The one-vs-all training uses 80% of the samples training and the remaining 20% for testing and implements

cross validation to reduce bias. More precisely, the *repeated random subsampling validation* or Monte Carlo cross-validation approach of [36] has been applied. In this approach, random subsampling is performed *t* times (t=10 in this case) and average values of accuracy are calculated for each value of λ and subset of parameters. Note that the obtained accuracy value actually represents the percentage of samples that have been properly classified in each test.

At the end of the training process (which in effect considers $c \cdot L$ combinations of λ and parameter subsets), the value of λ and parameter subset that lead to the highest accuracy are selected. If more than one combination gives the same highest accuracy, the one with the lowest number of features is selected on the grounds that it will produce a simpler and faster classifier.

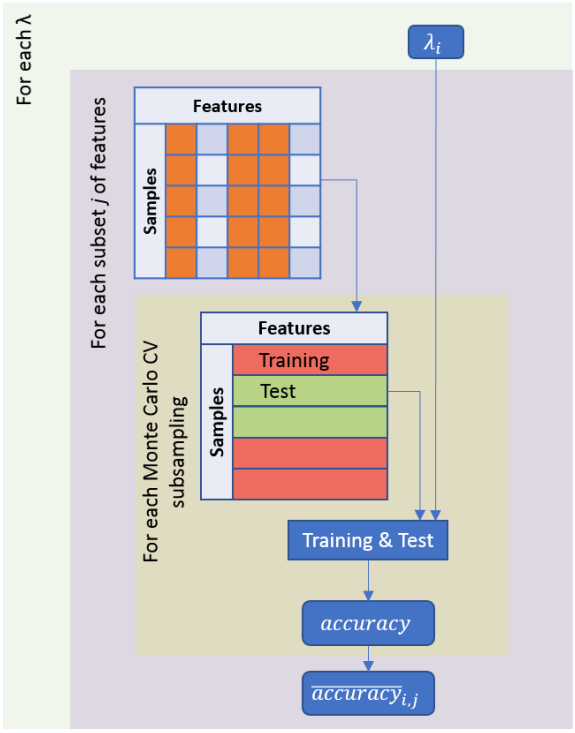

Figure 6: Strategy followed for parameters selection.

4 Experimental Results

4.1 Experimental case study

The approach presented in this paper has been tested with data from the main (south) façade of the Chapel Royal in Stirling Castle, Scotland, a category A listed building and a Scheduled Ancient Monument. It is located in the burgh of Stirling, Scotland. The listing description is limited but importantly asserts that it is rectangular in plan and was built in 1594. The South elevation façade fenestration is characterised by a '*Central doorway flanked by coupled columns; 3-2 light windows to either side*'. The façade is constructed of ashlar sandstone.

The masonry style is ashlar that is characterised as squared blocks with a finely tooled or polished face. Blonde sandstone forms the majority of the masonry walling material. Red sandstone mullions and margins to windows are noted forming the fenestration. Whilst some geological variability is

noted it is composed ostensibly of a fine-grained sandstone built in a lime ashlar mortar with an approximate joint width of 3mm. Geological variation is denoted by masonry colour and mineralogical change. Occasional plastic repair is noted and are particularly pronounced at the window margins.

Stirling Castle is generally heavily exposed to atmospheric conditions due to the inherent elevation of the site. The chapel is however offered shelter and some protection because of the position of surrounding structures [37] and the courtyard arrangement. This influences the severity of defects and rapidity of decay processes, noted due in part to lower moisture contents in the masonry.

4.2 Data acquisition and pre-processing

With respect to TLS data acquisition, four scans of the south façade of the Chapel Royal (Figure 7), were taken from strategic locations with a Leica Geosystems P40 TLS device. After a first alignment (i.e. roto-translation) of the obtained point clouds and a further fine registration, by means of an ICP algorithm [38], a dense point cloud containing 72 million points was produced for the façade (see Figure 8a). Colour information was added from a photogrammetric model produced as described below.

Figure 7: South façade of the Chapel Royal in Stirling Castle.

A photogrammetric (PG) model was created with 347 pictures taken by a Nikon D810 camera equipped with a 14mm Nikon lens. The coloured dense point cloud was generated through Structure from Motion techniques. The obtained point cloud was subsequently scaled and aligned to the TLS point cloud.

Colouring the TLS point cloud with the RGB data from the photogrammetric model was performed using the k-nearest neighbours (kNN) algorithm [39]. In this particular case, considering $k = 1$, every point in the TLS dataset was coloured with the RGB values of its nearest neighbour from the PG point cloud.

A Scan-vs-BIM process [40] was then employed with an HBIM model of the façade [24] to automatically segment the points belonging to the wall (and discarding those belonging to the windows and door). The result of this step is shown in Figure 8b. Finally, as described in Section 3.2, the segmentation process based on the analysis of data in the frequency domain was executed to identify the individual masonry units composing the wall. The final outcome, corresponding to the point cloud of ashlar masonry is illustrated in Figure 8c.

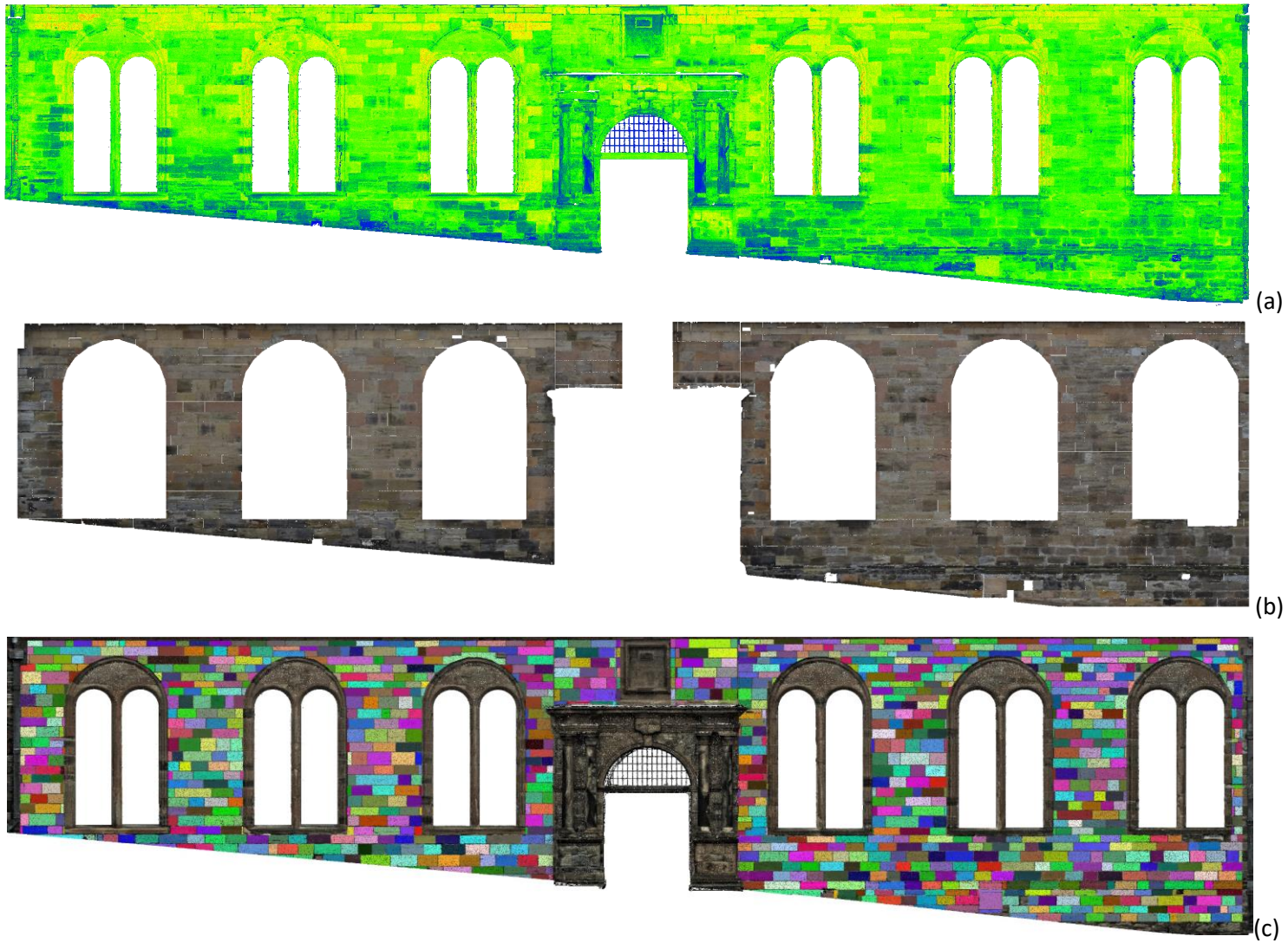

Figure 8: (a) Point cloud obtained from terrestrial laser scanning; (b) Point cloud coloured with photogrammetry RGB values; (c) Segmented ashlar point cloud.

4.3 Defect detection

After fitting a plane to the surface of each ashlar unit, as described in Section 3, areas with potential geometry-related defect manifestations were detected as connected components of outliers that are defined as the points further than 2.5mm from the fitted plane – 2.5mm was selected because 'polished' finishing had been identified in this façade. Figure 9a illustrates, highlighted in red, areas with potential geometry-related defect manifestations. As can be appreciated, the bottom part of the façade is potentially more affected by this kind of defect manifestations. A total of 3,383 areas have been detected covering 763 different ashlar units.

To detect areas with chromatic alterations that could be defect manifestations, colour data of each stone was processed as explained in Section 3.2. In Figure 9b, darker regions in ashlar units are plotted in red, whereas lighter areas are highlighted in pink. Although ashlar units from the top part of the façade seem to be less affected by chromatic alterations, there is not a region on the wall particularly altered by this kind of defects. In this case, 3,621 areas have been detected within 672 ashlar units.

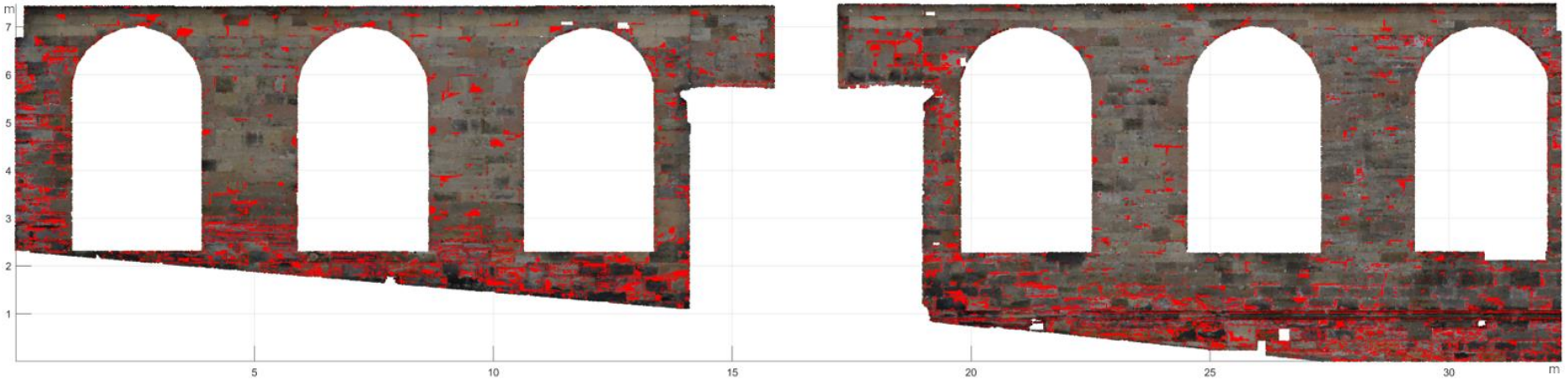

(a)

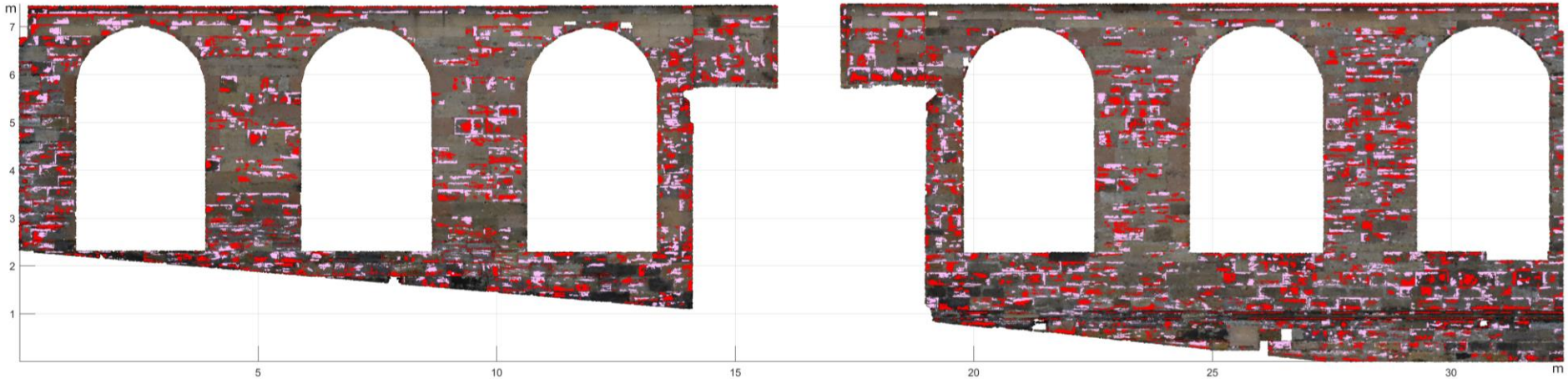

(b)

Figure 9: (a) Potential defective areas associated to geometry-related decay; (b) Areas with high variation of colour

4.4 Defect classification

4.4.1 Labelling and training

The left part of the south façade of the Chapel Royal was meticulously evaluated by expert surveyors, following traditional 'visual survey' techniques. In this work, around 500 deteriorated ashlar regions, containing almost 650 faults, were digitally labelled by the experts using a purpose-designed user interface. The number of instances of different defects is summarised in Figure 10, which shows that not all the defects are equally present on the evaluated wall. Erosion, mechanical damage, delamination and discolouration are the most prominent faults in the evaluated façade, representing more than 90% of the defective areas, and are thus in significant enough quantities to be considered in this study.

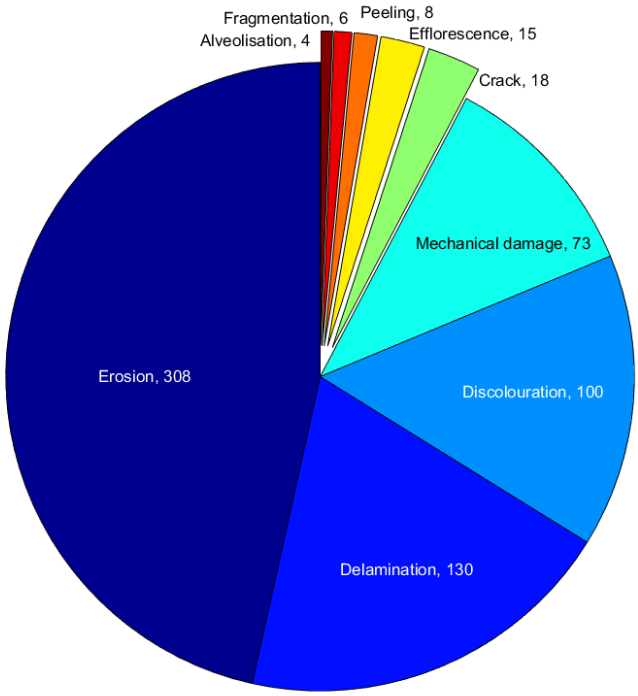

Figure 10: Distribution and frequency of labelled defective areas

It can be noted that delamination, erosion and mechanical damage are different cases of material loss, whereas discolouration is a chromatic alteration. Therefore, two different training and classification processes were performed: a first one dealing with geometry-related defects and a second one devoted to study discoloured areas.

As previously mentioned in Section 4, logistic regression algorithms were employed to discriminate between different defects. In the case of geometric deterioration patterns, a one-vs-all training process was performed, whereas a simpler strategy was followed for coloured-related defects since only a binary classification was needed to differentiate regions with colour alterations from those without defects.

4.4.1.1 Geometry-related defects

Amongst the samples labelled as 'erosion', 'delamination' and 'mechanical damage', 20 of each class were employed to test the classifier, following the Monte Carlo cross-validation previously detailed. The remaining samples were allocated for training purposes.

Additionally, 95 samples containing non-defective regions were extracted from the point cloud to create a "neutral" class. This class is of interest to classify, and subsequently revise, potentially incorrectly labelled areas. Table 3 details the distribution of labelled defects per operation.

Table 3: Distribution of labelled defects per ML operation

Defect	Training	Test
Erosion	262	20
Delamination	117	20
Mechanical damage	62	20
Non-defective	95	20

The selection of features to be used for the classifier was carried out by following the approach presented in Section 3.3.1. Five values of λ between 0.00375 and 5 were tested, and the 16 parameters enumerated in Table 4 were evaluated.

A total of 65,535 combinations (i.e. subsets) of features were processed, each of them for the 5 values of λ. The Monte Carlo cross-validation process was performed 10 times per subset of features and average values of accuracy were calculated to extract the optimal subset of features.

The structures delivered by the feature selection algorithm with the highest accuracy (69.25%), all obtained with a regularisation parameter $\lambda = 0.00375$, are listed in Table 4. From those, the one with fewest features was selected. Since there were two subsets with equal number of features, the one whose features were most repeated amongst the other subsets was selected (S4 in Table 4).

Table 4: Initial parameters for geometry related defects classification and subsets of features for highest accuracy values

ID	Parameter	S 1	S 2	S 3	S 4
1	Percentage of Inliers	✓	✓		✓
2	Mean of outliers' normal	✓		✓	
3	Standard Deviation of outliers' normal				
4	R_a (roughness coefficient)		✓	✓	✓
5	R_aO (roughness coefficient of outliers)	✓	✓		
6	Area of segment		✓	✓	✓
7	Area of all segments in ROI	✓	✓		✓
8	Elongation of segment	✓		✓	
9	Rectangleness of segment	✓	✓	✓	✓
10	Circularity of segment	✓	✓	✓	✓
11	Number of segments in ROI	✓	✓	✓	✓
12	Mean distance from outliers to fitted plane	✓			
13	Depth map contrast	✓	✓	✓	✓
14	Depth map correlation				
15	Depth map energy	✓	✓	✓	✓
16	Depth map homogeneity	✓	✓	✓	✓

Using these selected parameters and $\lambda = 0.00375$, Monte Carlo cross-validation was run 100 times and predictions corresponding to the average value of accuracy, for all the tests, were used to produce the confusion matrix shown in Table 5. Table 6 then reports the recall (Eq 12) and precision (Eq 13) values.

$$recall = \frac{TP}{TP+FN} \quad (12)$$

$$precision = \frac{TP}{TP+FP} \quad (13)$$

As can be seen in Table 5, erosion, mechanical damage and non-defective areas were predicted effectively, as illustrated in Table 6, after calculating recall (Eq 12) and precision (Eq 13) values. However, no delamination samples were successfully predicted. This is because delamination and erosion commonly appear together in this wall and, as a result, samples tend to be simultaneously labelled as 'delamination' and 'erosion', rendering their differentiation very challenging.

Table 5: Confusion matrix for the classification of geometry-related defects.

		Actual			
		Erosion	**Delamination**	**Mechanical damage**	**Non-defective**
Predicted	**Erosion**	18	19	4	2
	Delamination	0	0	0	0
	Mechanical damage	0	0	16	0
	Non-defective	2	1	0	18

Table 6: Recall and precision coefficients for geometry-related defects.

Defect	**Recall**	**Precision**
Erosion	0.9	0.42
Delamination	0	-
Mechanical damage	0.8	1
Non-defective	0.9	0.86

4.4.1.2 Discolouration

Regarding the training of the classifier to discriminate areas affected by discolouration, similarly to the evaluation of geometry-related defects, more than 100 samples were randomly selected that had no colour alteration and were used as inputs to the algorithm together with the datasets from the areas labelled as 'discoloured'. Here as well, 20 samples were used for testing, with the resulting distribution of samples as per the process shown in Table 7.

Table 7: Distribution of labelled colour-related defects per ML operation

Defect	**Training**	**Test**
Discolouration	80	20
Non-defective	115	20

Similarly to the parameter selection process detailed in the previous subsection, five values of λ between 0.00375 and 5 were tested, and the 17 parameters enumerated in Table 8 were evaluated.

A total of 131,071 combinations (i.e. subsets) of features were evaluated, each of them for the 5 values of λ. The Monte Carlo cross-validation process was performed 10 times per subset of features and average values of accuracy were calculated to extract the optimal subset of features.

The only structure delivered by the feature selection algorithm with the highest accuracy (100%), obtained with $\lambda = 0.00375$, is listed in Table 8. The parameters summarised in the table are, therefore, selected as features to the classifier.

Table 8: Initial parameters for colour related defects classification and subset of features for highest accuracy value

ID	Parameter	Subset
1	Range of hue	
2	H_σ	
3	Range of value	✓
4	V_σ	
5	Skewness	✓
6	Hue map contrast	✓
7	Hue map correlation	
8	Hue map energy	
9	Hue map homogeneity	
10	Value map contrast	
11	Value map correlation	
12	Value map energy	
13	Value map homogeneity	✓
14	Gray map contrast	✓
15	Gray map correlation	
16	Gray map energy	
17	Gray map homogeneity	

After running the Monte Carlo cross validation 100 times, results for the classification of samples labelled as 'discolouration' and 'non-defective' are presented in Table 9. In this case, discoloured areas were correctly discriminated from those not containing chromatic alterations. Table 10 summarises the recall and precision values for this classification process.

Table 9: Confusion matrix for the classification of discoloured areas

		Actual	
		Discolouration	**Non-defective**
Predicted	**Discolouration**	19	0
	Non-defective	1	20

Table 10: Recall and precision coefficients for colour related defects

Defect	Recall	Precision
Discolouration	0.95	1
Non-defective	1	0.95

4.4.2 Classifying potentially affected areas

Once the classifiers were trained and validated, they were used to categorise the potentially affected areas which were previously automatically detected, as reported in section 4.3.

For each of those detected regions, the selected geometric and colour-related parameters were calculated and used as features to the designed logistic regression classifier. Figure 11 illustrates the results after classification of defective areas.

Figure 11a shows, highlighted in red, the areas potentially affected by erosion. As can be seen, the bottom part of the wall is the most affected region. Also, the left and right ends of the walls have decayed regions. These defective areas are most likely attributed to salt crystallisation and freeze-thaw low magnitude spalling.

Figure 11b shows, in green, several regions potentially affected by mechanical damage. As can be appreciated, most of them are at similar height and present the same shape and size. This is consistent with the fact that, in the experts' opinions, these are the results of musket shots.

With respect to chromatic alterations on stone, numerous regions were identified by the classifier as potentially affected by discolouration (see Figure 11c). As previously mentioned for erosion-affected areas, this kind of deterioration can be related to the effect of salts on the stone.

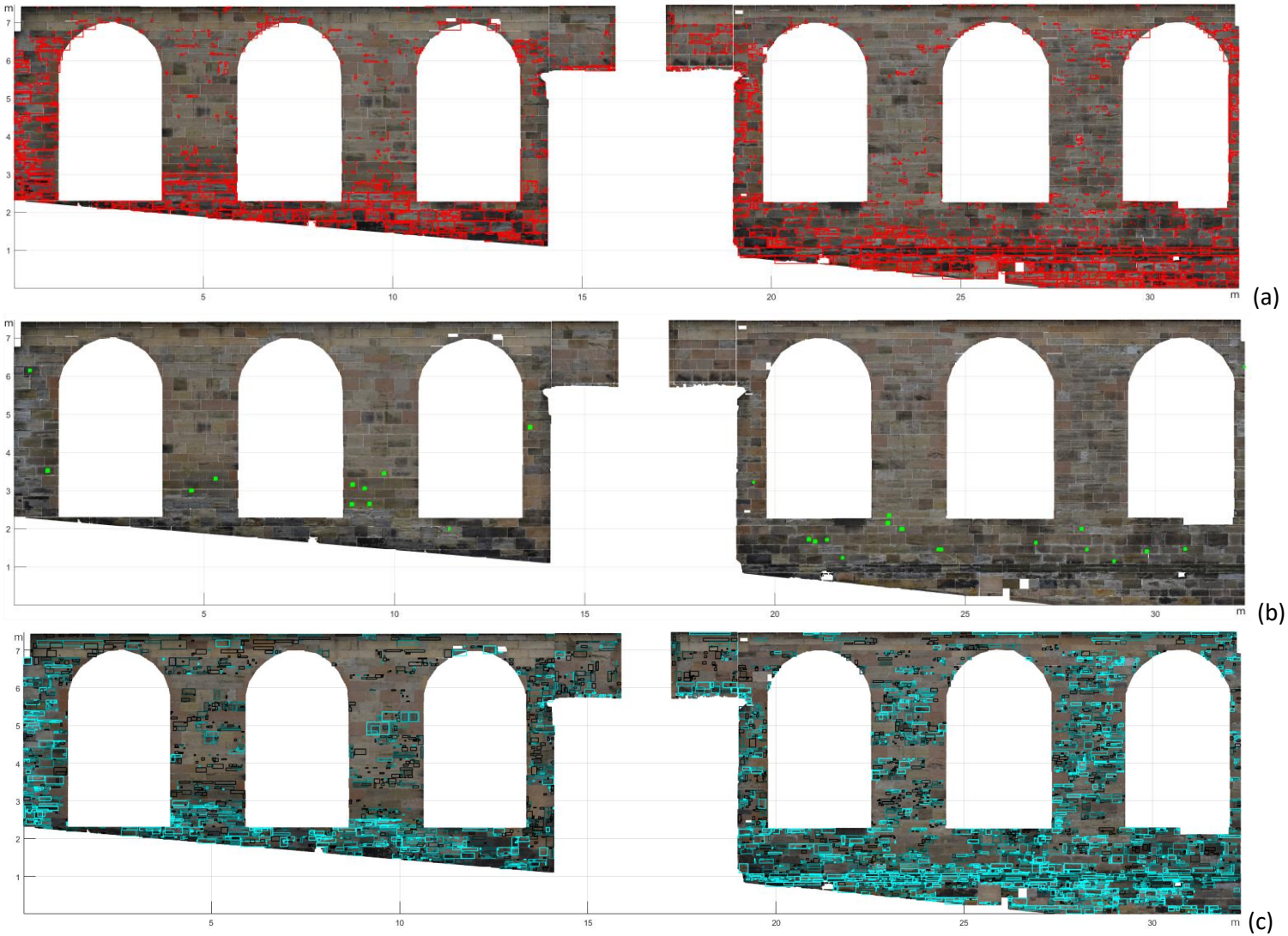

Figure 11: (a) Areas classified as potentially affected by erosion; (b) Areas classified as potentially affected by mechanical damage; (c) Areas classified as potentially affected by discolouration (lighter rectangles correspond to more confidently labelled areas)

5 Conclusions and future works

A new strategy for detecting and classifying deterioration patterns on ashlar masonry walls is presented in this paper. After TLS and PG data acquisition and subsequent segmentation of the obtained point cloud into individual stones, various parameters are calculated for individual ashlar units aiming to identify defective areas. These parameters, related to both geometry and colour information, are subsequently evaluated and used as input features to a machine learning algorithm.

As the experiments show, favourable results are obtained for the detection and classification of discolouration patterns on the wall. In the case of the classification of geometry-related defects, delamination patterns have been confused with erosion. It must be emphasised that these two defects commonly appear together, and even expert surveyors can have difficulties discriminating between them. Further research should nonetheless be devoted to a deeper evaluation of these two types of defects.

This unit and sub-unit level information, which is obtained after the segmentation and defect classification processes, can be included in BIM models to effectively: record and retrieve survey information over time; and monitor and communicate about particular masonry regions affected by various defects. In future works, it is proposed to study supra-unit regions.

Subjectivity in visual surveying tasks can lead to biased evaluations of defective masonry, providing outcomes strongly influenced by the specialist's background and experience. This can also affect machine learning processes, producing insufficiently/incorrectly trained algorithms. Therefore, collaborative labelling of defective areas by a team of surveyors, with different points of views and opinions, can help generate more robust classifiers, delivering more reliable results.

In a similar manner, the nature of defects is distinct for different materials, shape and finishing of masonry units as well as the history of the building. Future works will pursue the digital recording of spatial data from several historic buildings and the labelling of different kinds of masonry (e.g. coursed and random rubble) to cover a wider extent of stone works. A larger labelled dataset would also support the investigation of Deep Learning approaches to defect detection and classification. The application of the method will also be further tested and validated adopting a wider range of building professionals including: building surveyors, architects and other conservation specialists.

As an extension of the approach proposed in this paper, both segmentation and defect detection and classification outcomes will be used to improve the level of detail (in terms of geometry, as well as material interfaces and characteristics) of numerical models employed in finite elements analysis (FEA), so that structural performance can be characterised more reliably (see [41] as an example of related work).

Acknowledgements

This paper was made possible thanks to research funding from Historic Environment Scotland (HES). The views and opinions expressed in this article are those of the authors and do not necessarily reflect the official policy or position of HES. The authors would also like to acknowledge the HES Digital Documentation team for providing us with the point cloud data used in the experiments reported in this paper.

References

[1] British Standards Institution. (2013) BS 7913 'The principles of the conservation of historic buildings', ISBN 978 0 580 75778 5.

[2] Cecchi, R. and Gasparoli, P. (2012) Preventive and planned maintenance of protected buildings: methodological tools for the development of inspection activities and maintenance plans Alinea Editrice. Firenze, 2012. ISBN 978 8 860 55689 9.

[3] Forster A.M. and Carter, K. (2011) A framework for specifying lime mortars for rubble masonry construction. Structural Survey: Journal of Building Pathology & Refurbishment 29(5), 373-396. https://doi.org/10.1108/02630801111182411

[4] Straub, A. (2009) Dutch standard for condition assessment of buildings. Structural Survey, Vol. 27 No. 1, pp. 23-35. https://doi.org/10.1108/02630800910941665

[5] Forster A.M. and Douglas, J.E. (2010) Condition survey objectivity & philosophy driven masonry repair: An increased probability for project divergence? Structural Survey: Journal of Building Pathology & Refurbishment 28(5), 384-407. https://doi.org/10.1108/02630801011089173

[6] Ogleby, C. L. (1995) Advances in the digital recording of cultural monuments. ISPRS Journal of Photogrammetry and Remote Sensing, 50(3), 8-19. https://doi.org/10.1016/0924-2716(95)91286-S.

[7] Bosché, F., Forster, A. and Valero, E. (2015) 3D surveying technologies and applications: point clouds and beyond. Technical Report. Heriot-Watt University, Edinburgh, 2015. url: https://cyberbuild.hw.ac.uk/publications/report/Bosche-2015-Report.pdf (Accessed 20/05/19)

[8] Valero, E., Bosché, F., Forster, A., Wilson, L. and Leslie, A. (2016) Comparison of 3D Reality Capture Technologies for the Survey of Stone Walls. Arqueológica 2.0. Valencia (Spain), September 2016. https://doi.org/10.4995/arqueologica8.2015.2582.

[9] Wilson, L., Rawlinson, A., Mitchell, D. et al. (2013) The Scottish Ten Project: Collaborative Heritage Documentation. The International Archives of the Photogrammetry, Remote Sensing and Spatial Information Sciences, XL-5/W2, 685-690.. https://doi.org/10.5194/isprsarchives-XL-5-W2-685-2013.

[10] Scandurra, S., Pulcrano, M., Tarantino, C. and Di Luggo, A. (2017) H-BIM Modeling and Historical Reconstruction of Architectural Heritage. Building Information Modeling, Data & Semantics, 1, October 2017, ISSN 26108755. url: http://www.dienne.org/en/2018/10/13/scandurra-eng/ (Accessed 10/05/19)

[11] ICOMOS-ISCS. (2008) Illustrated Glossary on Stone Deterioration Patterns. ICOMOS International Scientific Committee for Stone (ISCS). Champigny/Marne, France, September 2008. ISBN: 978-2-918086-00-0.

[12] Quattrini, R., Pierdica, R., Morbidoni, C. and Maliverni, E. S. (2017) Conservation-Oriented HBIM. The BIMEXPLORER web tool. The International Archives of the Photogrammetry, Remote Sensing and Spatial Information Sciences, Volume XLII-5/W1, 2017. GEOMATICS & RESTORATION – Conservation of Cultural Heritage in the Digital Era, 22–24 May 2017, Florence, Italy. https://doi.org/10.5194/isprs-archives-XLII-5-W1-275-2017.

[13] De Matías, J., Berenguer, F., Cortés, J.P., De Sanjosé, J. J. and Atkinson, A. (2013) Laser Scanning for the Geometric Study of the Alcantara Bridge and Coria Cathedral. The International Archives of the Photogrammetry, Remote Sensing and Spatial Information Sciences, Volume XL-5/W1, 2013 3D-ARCH

2013 - 3D Virtual Reconstruction and Visualization of Complex Architectures, 25 – 26 February 2013, Trento, Italy. https://doi.org/10.5194/isprsarchives-XL-5-W1-51-2013.

[14] Wilson, L., Rawlinson, A., Frost, A. and Hepher, J. (2018) 3D digital documentation in disaster management for historic buildings: Applications in the aftermath of the Mackintosh building fire at The Glasgow School of Art, Journal of Cultural Heritage 31: 24-32. https://doi.org/10.1016/j.culher.2017.11.012

[15] Cardaci, A., Mirabella Roberti, G. and Versaci, A. (2011) From the Continuous to the Discrete Model: A Laser Scanning Application to Conservation Projects. In Proceedings of the Congress of the International Society for Photogrammetry and Remote Sensing (ISPRS), pages 437–444, 2011. https://doi.org/10.5194/isprsarchives-XXXVIII-5-W16-437-2011.

[16] Bruno, F., Bianco, G., Muzzupappa, M., Barone, S. and Razionale, A.V. (2011) Experimentation of Structured Light and Stereo Vision for Underwater 3D Reconstruction. ISPRS Journal of Photogrammetry and Remote Sensing, 66(4):508 – 518, 2011. https://doi.org/10.1016/j.isprsjprs.2011.02.009.

[17] Temizer, T. Nemli, G., Ekizce, E., Ekizce, A., Demir, S., Bayram, B., Askin, F.H., Cobanoglu, A. V. and Yilmaz, H. F. (2013) 3D Documentation of a Historic Monument Using Terrestrial Laser Scanning Case Study: Byzantine Water Cistern, Istanbul. The International Archives of the Photogrammetry, Remote Sensing and Spatial Information Sciences, Volume XL-5/W2, 2013 XXIV International CIPA Symposium, pages 623–628, Strasbourg, France, 2013. https://doi.org/10.5194/isprsarchives-XL-5-W2-623-2013.

[18] Antón, D., Medjdoub, B., Shrahily, R. and Moyano, J. (2018) Accuracy evaluation of the semi-automatic 3D modeling for historical building information models, International Journal of Architectural Heritage, Volume 12, Issue 5, 2018. https://doi.org/10.1080/15583058.2017.1415391.

[19] Chiabrando, F., Lo Turco, M. and Santagati, C. (2017) Digital Invasions: from Point Clouds to Historical Building Object Modelling (H-BOM) of a UNESCO WHL Site. The International Archives of the Photogrammetry, Remote Sensing and Spatial Information Sciences, Volume XLII-2/W3, 2017. 3D Virtual Reconstruction and Visualization of Complex Architectures, 1–3 March 2017, Nafplio, Greece. https://doi.org/10.5194/isprs-archives-XLII-2-W3-171-2017.

[20] Pöchtrager, M., Styhler-Aydın, G., Döring-Williams, M. and Pfeifer, N. (2017) Automated Reconstruction of Historic Roof Structures from Point Cloud – Development and Examples. ISPRS Annals of the Photogrammetry, Remote Sensing and Spatial Information Sciences, Volume IV-2/W2, 2017 26th International CIPA Symposium 2017, 28 August–01 September 2017, Ottawa, Canada. http://doi.org/10.5194/isprs-annals-IV-2-W2-195-2017

[21] Cappellini, V., Stefani, C., Nony, N. and De Luca, L. (2012) Surveying Masonry Structures by Semantically Enriched 2.5D Textures: A New Approach. In Marinos Ioannides, Dieter Fritsch, Johanna Leissner, Rob Davies, Fabio Remondino, and Rossella Caffo, editors, Progress in Cultural Heritage Preservation, volume 7616 of Lecture Notes in Computer Science, pages 729–737. Springer Berlin Heidelberg, 2012. https://doi.org/10.1007/978-3-642-34234-9_77

[22] Valero, E., Bosché, F., Forster, A., Wilson, L., and Leslie, A. (2017) Evaluation of Historic Masonry Substrates: Towards Greater Objectivity and Efficiency – in Heritage Building Information Modelling, Routledge. ISBN 9781138645684.

[23] Valero, E., Bosché, F. and Forster, A. (2018) Automatic Segmentation of 3D Point Clouds of Rubble Masonry Walls, and its Application to Building Surveying, Repair and Maintenance. Automation in Construction. 96, pages 29-39. https://doi.org/10.1016/j.autcon.2018.08.018

[24] Valero, E., Forster, A., Bosché, F., Renier, C., Hyslop, E. and Wilson, L. (2018) High Level-of-Detail BIM and Machine Learning for Automated Masonry Wall Defect Surveying. Proceedings of the 35th International Symposium on Automation and Robotics in Construction (ISARC), 2018, Berlin, Germany. https://doi.org/10.22260/ISARC2018/0101.

[25] Oses, N. and Dornaika, F. (2013) Image-Based Delineation of Built Heritage Masonry for Automatic Classification. In Mohamed Kamel and Aurélio Campilho, editors, *Image Analysis and Recognition*, volume 7950 of *Lecture Notes in Computer Science*, pages 782–789. Springer Berlin Heidelberg, 2013. https://doi.org/10.1007/978-3-642-39094-4_90.

[26] Armesto-González, J., Riveiro-Rodríguez, B., González-Aguilera, D. and Rivas-Brea, M.T. (2010) Terrestrial laser scanning intensity data applied to damage detection for historical buildings. Journal of Archaeological Science, Volume 37, Issue 12, 2010, Pages 3037-3047, ISSN 0305-4403, https://doi.org/10.1016/j.jas.2010.06.031.

[27] Sánchez-Aparicio, L. J., Del Pozo, S., Ramos, L. F., Arce, A. and Fernandes, F. M. (2018) Heritage site preservation with combined radiometric and geometric analysis of TLS data. Automation in Construction, 85, 24-39, 2018, https://doi.org/10.1016/j.autcon.2017.09.023.

[28] Moussa, W. (2014) Integration of Digital Photogrammetry and Terrestrial Laser Scanning for Cultural Heritage Data Recording. PhD thesis. Deutsche Geodatische Kommission der Bayerischen Akademie der Wissenschaften, Munich, Germany. ISBN: 978-3-7696-5137-9.

[29] Warland E. G. (1929) Modern Practical Masonry. B.T Batsford, London, 1929. ISBN: 978-1873394762.

[30] Joblove, G. H. and Greenberg, D. (1978) Color Spaces for Computer Graphics, Proceedings of the 5th Annual Conference on Computer Graphics and Interactive Techniques, SIGGRAPH '78, New York, USA. https://doi.org/10.1145/800248.807362.

[31] Smith, A. R. (1978) Color Gamut Transform Pairs. Proceedings of the 5th Annual Conference on Computer Graphics and Interactive Techniques, SIGGRAPH '78, New York, USA. https://doi.org/10.1145/965139.807361.

[32] Haralick, R.M., Shanmugan, K. and Dinstein, I. (1973) Textural Features for Image Classification. IEEE Transactions on Systems, Man, and Cybernetics, Vol. SMC-3, 1973, pp. 610-621. https://doi.org/10.1109/TSMC.1973.4309314.

[33] Haralick, R.M. and Shapiro, L. G. (1992) Computer and Robot Vision. Addison-Wesley Longman Publishing Co., Inc. Boston, MA, USA. 1992. ISBN: 978-0201108774.

[34] Joanes, D. N. and Gill, C. A. (1998) Comparing measures of sample skewness and kurtosis. Journal of the Royal Statistical Society (Series D): The Statistician. 47 (1): 183–189. https://doi.org/10.1111/1467-9884.00122.

[35] Mohri, M., Rostamizadeh, A. and Talwalkar, A. Foundations of Machine Learning. The MIT Press, Cambridge, Massachusetts, 2012. ISBN: 978-0262039406.

[36] Dubitzky, W., Granzow, M. and Berrar, D. (2007) Fundamentals of data mining in genomics and proteomics. Springer Science & Business Media. p. 178. ISBN: 978-0-387-47509-7.

[37] British Standards Institution (1995) BS 6399 'Loading for Buildings – Part 2: Code of Practice for Wind Loads', ISBN: 0 580 27447 0.

[38] Besl, P.J. and McKay, N.D. (1992) Method for registration of 3-D shapes, IEEE Transactions on Pattern Analysis and Machine Intelligence. Vol. 14 (2) (1992) 239–256, https://doi.org/10.1109/34.121791.

[39] Friedman, J. H., Bentely, J. and Finkel, R. A. (1977) An Algorithm for Finding Best Matches in Logarithmic Expected Time. ACM Transactions on Mathematical Software. Vol. 3, Issue 3, 1977, pp. 209–226. https://doi.org/10.1145/355744.355745.

[40] Bosché, F., Guillemet, A., Turkan, Y. and Haas, C.T. (2013) Tracking the Built Status of MEP Works: Assessing the Value of a Scan-vs-BIM System. Journal of Computing in Civil Engineering, 28(4), 2013. https://doi.org/10.1061/(ASCE)CP.1943-5487.000034.

[41] D'Altri, A.M., Milani, G., de Miranda, S., Castellazzi, G., Sarhosis, V. (2018) Stability analysis of leaning historic masonry structures. Automation in Construction, vol. 92, August 2018. https://doi.org/10.1016/j.autcon.2018.04.003.